THE JOURNAL OF BIOLOGICAL CHEMISTRY VOL. 289, NO. 44, pp. 30645–30656, October 31, 2014

Dynamin-related Protein 1 (Drp1) Promotes Structural Intermediates of Membrane Division*[S]

Received for publication, April 22, 2014, and in revised form, September 17, 2014 Published, JBC Papers in Press, September 18, 2014, DOI 10.1074/jbc.M114.575779

Begoña Ugarte-Uribe[‡§], **Hans-Michael Müller**[¶], **Miki Otsuki**[‡], **Walter Nickel**[¶], **and Ana J. García-Sáez**[‡§1]

From the [‡]*Max-Planck Institute for Intelligent Systems, 70569 Stuttgart, Germany, the* [§]*Interfaculty Institute of Biochemistry, University of Tübingen, 72076 Tübingen, Germany, and the* [¶]*Heidelberg University Biochemistry Center, 69120 Heidelberg, Germany*

Background: Drp1 mediates mitochondrial division via a poorly understood mechanism.
Results: Drp1 promotes giant vesicle tethering and concentrates at contact sites in structures similar to those found in dividing mitochondria.
Conclusion: Besides membrane constriction, Drp1 stabilizes structural intermediates of membrane division.
Significance: This new role of Drp1 helps us understand mitochondrial biology.

Drp1 is a dynamin-like GTPase that mediates mitochondrial and peroxisomal division in a process dependent on self-assembly and coupled to GTP hydrolysis. Despite the link between Drp1 malfunction and human disease, the molecular details of its membrane activity remain poorly understood. Here we reconstituted and directly visualized Drp1 activity in giant unilamellar vesicles. We quantified the effect of lipid composition and GTP on membrane binding and remodeling activity by fluorescence confocal microscopy and flow cytometry. In contrast to other dynamin relatives, Drp1 bound to both curved and flat membranes even in the absence of nucleotides. We also found that Drp1 induced membrane tubulation that was stimulated by cardiolipin. Moreover, Drp1 promoted membrane tethering dependent on the intrinsic curvature of the membrane lipids and on GTP. Interestingly, Drp1 concentrated at membrane contact surfaces and, in the presence of GTP, formed discrete clusters on the vesicles. Our findings support a role of Drp1 not only in the formation of lipid tubes but also on the stabilization of tightly apposed membranes, which are intermediate states in the process of mitochondrial fission.

Mitochondria are essential organelles within the cell that host key metabolic reactions and cellular processes, including biosynthetic events, respiration, calcium homeostasis, and the intrinsic pathway of apoptosis (1, 2). Mitochondria form branched and tubular networks that undergo continuous fission and fusion (3). The balance between these counteracting processes is essential for the maintenance of a functional mitochondrial structure and plays a role in mitochondrial biogenesis and metabolism, in mitophagy, and in neurodegenerative diseases (4–6). On the other hand, peroxisomes are ubiquitous subcellular organelles that participate in a variety of important catabolic and anabolic functions, including hydrogen peroxide and lipid metabolism (7). It is thought that peroxisome proliferation also occurs by division, comprising three stages: elongation, constriction, and fission (8).

Dynamin-related protein (Drp1), an 80-kDa mechanochemical GTPase of the dynamin superfamily, is required for both mitochondrial and peroxisomal fission in mammals (9, 10). This protein shuttles between the cytosol and these organelles, where it is recruited to potential fission sites. Drp1 then oligomerizes at some of these foci, leading to membrane scission (9). Mitochondrial fission has mostly been studied in yeast, where the Drp1 homolog Dnm1 interacts with a mitochondrial fission adaptor (*i.e.* the fungus-specific adaptor mitochondrial division protein 1 (Mdv1) or its paralogue Caf4), which, in turn, binds to the tail-anchored fission protein 1 (Fis1) (11–14). However, mitochondrial division in mammals is believed to differ from that reported for yeast because homolog adaptor proteins are missing in mammals. Instead, new adaptors have been identified for Drp1 on mitochondrial and peroxisomal surfaces. Some of these adaptors are found in both mitochondria and peroxisomes, such as human fission protein 1 (hFis1) and mitochondrial fission factor (Mff) (15–17), whereas others are only located at the mitochondrial outer membrane, such as mitochondrial dynamic proteins of 49 and 51 kDa (MiD49/MiD51) (18–21).

Despite the identification of new mediators involved in mitochondrial fission, the molecular details of how Drp1 itself mediates membrane division in either mitochondria or peroxisomes remain poorly understood. Much of what is accepted in current models has been extrapolated from yeast Dnm1 and other dynamin family members (13, 22–25). Recent structural studies have revealed a novel assembly surface in the stalk of Drp1, termed interface 4 (26). This interface is thought to be necessary to assemble two neighboring Drp1 filaments, similar to the model proposed for yeast Dnm1 by EM reconstructions, where a broader filament size and different oligomer architectures were achieved compared with dynamin (23). Accordingly, Drp1 would mediate membrane constriction by GTP-dependent dynamic rearrangements of double filaments across helical turns (27, 28). A number of attempts have also been made in

* This work was supported by the Max Planck Society, by the German Cancer Research Center, and by German Ministry for Education and Research (BMBF) Grant N.0312040.
[S] This article contains supplemental Movie S1.
[1] To whom correspondence should be addressed: Interfaculty Institute of Biochemistry, Hoppe-Seyler-Str. 4, 72076 Tübingen, Germany. Tel.: 49-7071-29-73318; Fax: 49-7071-29-35296; E-mail: ana.garcia@uni-tuebingen.de.

reconstituted systems to unravel the GTPase and membrane remodeling activity of Drp1 (26, 29–32). For example, Drp1 self-assembly into rings and spirals in the absence of lipids is affected by the presence of MiD49 or MiD51 (31, 33). However, the ability of Drp1 to mediate membrane constriction remains under debate because assembly around liposomes and membrane tubulation have mainly been reported for pure phosphatidylserine membranes under the harsh conditions of electron microscopy (26, 31). Additional approaches that provide insight into the dynamic aspects of membrane remodeling by Drp1 under near-physiological conditions will be essential to understand the molecular mechanisms behind this process.

In this work, we reconstituted the membrane activity of Drp1 in a synthetic system on the basis of giant unilamellar vesicles (GUVs).[2] This allowed both direct visualization and quantification of the membrane remodeling action of Drp1 under chemically controlled conditions. In addition, we quantified the effect of lipid composition and GTP on Drp1 activity in large unilamellar vesicles (LUVs) by flow cytometry. Using lipid compositions mimicking the mitochondrial membrane and physiological buffers, we found that fluorescently labeled Drp1 bound to both curved and flat membranes, which sets it apart from other dynamin homologs. Drp1 induced the formation of lipid tubes depending on protein concentration, where cardiolipin seemed to be a potent stimulator. These findings are in agreement with the proposed constriction activity of Drp1 on mitochondrial membranes. Interestingly, Drp1 also promoted vesicle tethering and concentrated at the membrane contact sites, which are structural intermediates in the molecular pathway of membrane division likely involving non-lamellar lipid arrangements. In agreement with this, lipids with negative intrinsic monolayer curvature increased Drp1 membrane tethering activity. Similarly, we observed comparable tethered structures in living cells during Drp1-mediated mitochondrial division, in agreement with previous results in mammal and yeast cells (9, 13, 22, 31, 34). Together, our findings support a molecular mechanism by which Drp1 promotes membrane fission by stabilizing membrane topologies involved in membrane fission.

EXPERIMENTAL PROCEDURES

Drp1 Purification and Labeling—pCal-n-EK-Drp1 (isoform1) and pCal-n-EK-Drp1^{K38A} constructs were provided by Dr. C. Blackstone (Cell Biology Section, Neurogenetics Branch, National Institute of Neurological Disorders and Stroke, National Institutes of Health, Bethesda) (35, 36). *Escherichia coli* BL21 (DE3)-RIPL cells containing pCal-n-EK-Drp1 and pCaL-n-EK-Drp1^{K38A} were grown at 37 °C in Luria broth medium containing antibiotics until an A_{600} of ~0.6. protein expression was induced with 1 mM isopropyl 1-thio-β-d-galactopyranoside at 14 °C for 18 h. Cells pellets were resuspended in 25 mM Hepes (pH 7.4), 250 mM NaCl, 2 mM $CaCl_2$, 5 mM $MgCl_2$ and 1 mM imidazole containing 1 μg/ml DNase and protease inhibitors (Complete; EDTA-free Protease Inhibitor Mixture; Roche Applied Science), homogenized, and centrifuged at 20,000 × *g* for 40 min. The supernatant was affinity-purified using calmodulin affinity resin (Agilent/Stratagene). The fusion proteins calmodulin binding protein-Drp1 and -Drp1^{K38A} (called Drp1 and Drp1^{K38A} from this point on) were eluted from the resin with 25 mM Hepes (pH 7.4), 250 mM NaCl, and 10 mM EGTA and dialyzed overnight at 4 °C with 25 mM Hepes (pH 7.4), 500 mM NaCl, and 2 mM $MgCl_2$. Protein quality was checked by SDS-PAGE, and protein concentration was quantified by Bradford assay. Purified protein was stored with 50% (v/v) glycerol. Alexa Fluor 488 C_5 maleimide (Invitrogen) was covalently attached to cysteines in Drp1 and Drp1^{K38A} bound to the resin as described by the manufacturer. When formed, the Drp1-Alexa Fluor 488 bond cannot be cleaved by reducing agents. Excess of label was removed by washing. The labeling efficiency of the purified proteins was ~20% (1 mol of dye/5 mol of protein).

Drp1 Characterization in Native Gels—Purified Drp1 and Drp1^{K38A} samples were analyzed by 4–16% NativePAGE™ BisTris gel (Novex, Invitrogen) as described by the manufacturer.

GTPase Activity Assay—The GTPase activity of Drp1 was assayed using a colorimetric assay as described previously by Leonard *et al.* (37). Briefly, for GTPase assays of purified Drp1 samples (either unlabeled or Alexa Fluor 488-labeled samples), 0.5–0.6 μM Drp1 was added to 0.5 mM GTP (or as indicated) over a 5- to 90-min time course at 37 °C in 20 mM Hepes (pH 7.4), 150 mM KCl, 2 mM $MgCl_2$, and 1 mM DTT. Reactions were stopped at the indicated times by diluting 20 μl of the sample in 100 mM EDTA (final concentration) in a microtiter plate. Samples were then incubated with 150 μl of malachite green stock solution (1 mM malachite green and 10 mM ammonium molybdate in 1 N HCl), and the absorbance at 620 nm was determined using an Infinite M200 microplate reader (Tecan, Mainz, Germany). The k_{cat} and the substrate concentration at which velocity is half maximal ($k_{0.5}$) were calculated in GraphPad Prism using nonlinear regression curve fitting.

Drp1 Binding to GUVs—GUVs were produced by electroformation (38). The desired lipid mixture in chloroform was dried on platinum wires, which were immersed in 300 mM sucrose in the electroformation chamber, and electroformation proceeded for 2 h at 10 Hz at room temperature, followed by 1 h at 2 Hz. LabTec chambers (Nunc) were blocked with bovine serum albumin before mixing 300 μl of buffer (20 mM Hepes (pH 7.4), 150 mM KCl, and 1 mM $MgCl_2$) with the desired amount of Drp1. GUVs were added to the sample at a ratio of 80/300 μl. For Drp1-Al488, GUVs were first added to the chamber, followed by the addition of Drp1-Al488. Images were collected between 30 min or 1 h after incubation with the protein at 22 °C. More than 200 GUVs were analyzed for each sample.

Lipid Composition of GUVs—All lipids were from Avanti Polar Lipids. The lipid mixture mimicking the mitochondrial outer membrane composition, called here MLL, was prepared as in Ref. 39 with 46% egg L-α-phosphatidylcholine (PC), 25% egg L-α-phosphatidylethanolamine (PE), 11% bovine liver L-α-phosphatidylinositol (PI), 10% 18:1 phosphatidylserine (PS),

[2] The abbreviations used are: GUV, giant unilamellar vesicles; LUV, large unilamellar vesicles; MLL, mitochondrial-like lipids; PC, phosphatidylcholine; PE, phosphatidylethanolamine; PI, phosphatidylinositol; CL, cardiolipin; PG, phosphatidylglycerol; PA, phosphatidic acid; DiD, 1,1′-dioctadecyl-3,3,3′,3′ tetramethylindodicarbocyanine 4-chlorobenzenesulfonate salt.

and 8% cardiolipin (CL) (w/w) and variations of this as described. For fluorescence experiments, 0.1% (mol/mol) 1,1′-dioctadecyl-3,3,3′,3′ tetramethylindodicarbocyanine 4-chlorobenzenesulfonate salt (DiD) (Molecular Probes, Eugene, OR) was added to the lipid mixtures.

Confocal Microscopy—All images were acquired with a commercial LSM 710 microscope (Carl Zeiss, Jena, Germany). The excitation light was reflected by a dichroic mirror (MBS 488/561/633) and focused through a Zeiss C-Apochromat ×40, numerical aperture 1.2 water immersion objective onto the sample. The fluorescence emission was collected by the objective and directed by spectral beam guides to photomultiplier tube detectors. Images were processed with ImageJ.

Generation of LUVs—Briefly, five different lipid compositions were used for flow cytometry: MLL (PC:PE:Rhod-PE:PI:PS:CL (48.5:26.2:1:9.9:10.05:4.35) (mol:mol)), MLL PC (PC:PE:Rhod-PE:PI:PS (52.85:26.2:1:9.9:10.05) (mol:mol)), MLL PS (PC:PE:Rhod-PE:PI:PS (44.15:26.2:1:9.9:18.75) (mol:mol)), MLL PG (PC:PE:Rhod-PE:PI:PS:PG (44.15:26.2:1:9.9:10.05:8.7) (mol:mol)), and MLL PA (PC:PE:Rhod-PE:PI:PS:PA (44.15:26.2:1:9.9:10.05:8.7) (mol:mol)). In all cases, 2.5 mg of desired homogeneous lipid mixture film were rehydrated and homogenized in reconstitution buffer (25 mM HEPES (pH 7.4), 150 mM KCl, and 1 mM $MgCl_2$) with 10% sucrose (or GTPase buffer for GTPase assays). Following 10 cycles of freezing (liquid nitrogen) and thawing (37 °C, water bath), size extrusion using 400-nm filters was performed (LiposoFast-Basic, Avestin Inc., Canada).

Flow Cytometry—Liposomes were analyzed with a fluorescence-activated cell sorter Calibur instrument, and data were processed with CellQuest Pro software (BD Biosciences) and Flowing Software 2.5.1 (Cell Imaging Core, Turku Centre Biotechnology). Briefly, 1 mM liposomes were first blocked with 4% BSA for 1 h at 25 °C, washed, pelleted for 10 min at 16,000 × *g*, and resuspended in the same volume (resulting again in 1 mM liposome) of reconstitution buffer containing 500 nM Drp1-Al488 in the absence or presence of 1 mM GTP or GTP-γ-S. After 1 h incubation at 25 °C, samples were washed and measured (30,000 events). Each experiment was performed four times in duplicate. Raw data (fluorescent units) were used to calculate Drp1 binding per normalized liposomes (corrected fluorescence units) and membrane tethering (shape index) as described previously (40).

Cell Experiments—For live cell imaging, mouse embryonic fibroblast cells were transfected with Lipofectamine reagent (Invitrogen), the MitoDsRed plasmid, and the pEGFP-C1-Drp1 plasmid to visualize mitochondria and Drp1, respectively. The pEGFP-C1-Drp1 plasmid was provided by Dr. M. Jendrach (Experimental Neurology, Department of Neurology, University Medical School, Goethe University, Frankfurt am Main, Germany) (41). For endogenous Drp1 localization, HeLa cells were transfected with Mito-DsRed, fixed with 4% paraformaldehyde in PBS and immunostained with primary antibody against Drp1 (D6C7, Cell Signaling Technology) and an Atto488-coupled secondary antibody.

Statistical Analysis—All measurements were performed at least three times, and results are presented as mean ± S.D. Levels of significance were determined by two-tailed Student's *t* test, and a confidence level of greater than 95% ($p < 0.05$) was used to establish statistical significance.

RESULTS

Drp1 Labeling Does Not Significantly Alter Function—To ensure that the proteins used in this study retain their function, we characterized their GTPase activity and oligomeric state in solution. We first evaluated the assembly of purified Drp1 by native gel electrophoresis. In agreement with previous data (30, 35), unlabeled Drp1 was present mainly as tetramers (Fig. 1*A*). In the case of Drp1 labeled with Alexa Fluor 488, a fraction of dimeric Drp1 appeared besides the tetramers (Fig. 1*A*), probably because of the presence of reducing agents in the labeling reaction. Nevertheless, similar mixtures of dimers and tetramers have also been reported previously for active preparations of Drp1 (26, 36).

Higher order assembly of dynamins is required for maximal GTPase activity (22, 36, 42–44). This assembly can be promoted by lowering the ionic strength (22, 31, 36, 45). Taking this into account, we investigated Drp1-dependent GTP hydrolysis under conditions favoring non-assembly (500 mM KCl) or higher order self-assembly (50 mM KCl). As expected, Drp1 induced GTP hydrolysis in low ionic strength buffer but not under high ionic strength conditions (Fig. 1*B*). The catalytic parameters measured for Drp1 in the presence of 150 mM KCl, which mimics physiological conditions, were $k_{cat} = 7.051 \pm 0.2843$ min^{-1} and $k_{0.5} = 157.3 \pm 17.92$ μM. These values are similar to those reported previously for Drp1 under low ionic strength buffer (31) and for Dnm1 (14). In addition, self-assembly of dynamins can be stimulated by the presence of liposomes, thereby inducing enhanced GTPase activity (14, 26, 32, 46). To determine whether this is also the case for our purified Drp1, GTPase reactions were measured in the absence or presence of MLL LUVs, which mimic the lipid composition of the mitochondrial outer membrane. As expected, we detected enhanced GTPase activity in the lipid environment (1.42 ± 0.2-fold increase for unlabeled Drp1, $n = 3$ independent experiments) compared with the GTPase activity shown in the absence of liposomes (Fig. 1*C*). When Drp1 was fluorescently labeled, we also measured comparable GTPase activity in the absence of membranes, which was increased to a similar extent in samples containing liposomes when compared with unlabeled Drp1 (Fig. 1*C*). Together, these results suggest that neither the tag (calmodulin binding protein) present in the fusion protein nor fluorescent labeling interfere with Drp1 activity and membrane interactions.

Drp1 Promotes Lipid Tube Formation Independently of GTP—To gain insights into the molecular mechanism of Drp1-induced membrane division, we characterized the membrane activity of Drp1 in reconstituted membrane systems. To date, most used templates for studying Drp1 activity *in vitro* are on the basis of pure PS liposomes, which do not reproduce physiological conditions due to the fact that this lipid is nearly absent at the mitochondrion (~1 mol%) (47). Here we used GUVs as model membrane systems because they are free-standing membranes of several microns in size that allow chemical control of the lipid composition as well as direct, live visualization of Drp1 binding and membrane remodeling activity with con-

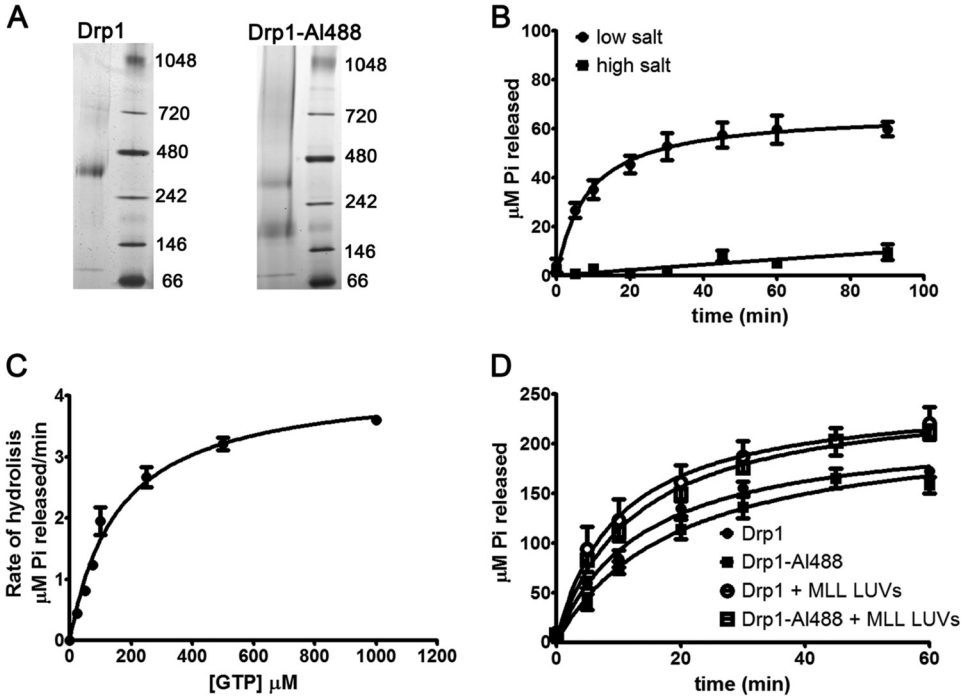

FIGURE 1. **Oligomeric state and GTPase activity of purified Drp1.** *A*, analysis of the oligomeric state of unlabeled (*left panel*) and Alexa Fluor 488-labeled (*right panel*) Drp1 assessed by native gels. *B*, time course of GTP hydrolysis by Drp1 (0.6 μM) measured in 0.1 mM GTP at 37 °C at low (50 mM KCl) and high (500 mM KCl) ionic strength. *C*, steady-state kinetics of Drp1 (0.5 μM) GTP hydrolysis measured at physiological ionic strength (150 mM KCl) and 37 °C. *D*, time course of GTP hydrolysis by unlabeled and Alexa Fluor 488-labeled Drp1 (0.5 μM) measured in 0.5 mM GTP at 37 °C at physiological (150 mM KCl) ionic strength in the absence or presence of MLL LUVs (0.05 mg/ml).

focal microscopy. In addition, to model the physiological conditions, we used GUVs mimicking the lipid composition of the mitochondrial outer membrane (MLL GUVs).

Immediately after mixing with GUVs in the observation chamber, Drp1 induced membrane tubulation and vesicle clustering in the absence of nucleotides (Fig. 2*A*). These membrane deformations were absent in control samples (Fig. 2*A*, top left panel) and increased with protein concentration (Fig. 2*A*, *bottom left panel* and *right panels*), indicating that Drp1 was responsible for this effect. We found that Drp1 promoted the formation of lipid tubes hundreds of micrometers long independently from the protein concentration tested (Fig. 2*A*, *right panels*). These membrane tubes were almost always connecting GUVs or bound to other tubes. The diameter of these tubes was around 200 nm or less and could not be accurately resolved by confocal microscopy because of the optical resolution limit. Unspecific lipid aggregates often appeared associated with the tubes. When analyzing the tubulation kinetics, tube growth was very fast, which made image collection very difficult. Nevertheless, we were able to image the process on a few occasions, for example as shown in supplemental Movie S1.

Drp1 Binds to Both Flat and Curved Membranes in Absence of Nucleotides—To visualize the localization of Drp1 during its membrane remodeling activity in GUVs, we used Drp1-Al488. As expected, fluorescently labeled Drp1 showed similar membrane remodeling compared with unlabeled Drp1 (Fig. 2*B*).

Upon incubation with the MLL GUVs, we observed immediate binding of Drp1-Al488 to the membrane, as shown by the increase in fluorescence intensity at the vesicle rim (Fig. 2*B*). Interestingly, the Drp1-Al488 signal was comparable on the GUV surface and on the lipid tubes, which indicates no significant preferential partitioning between the two structures (Fig. 2*B*). These results show that Drp1 has no preference for binding to curved or flat membranes, in contrast to what has been reported for other dynamins (48). In general, the distribution of the protein was mostly homogeneous on the membrane surface (Fig. 2*B*), suggesting that membrane association in the absence of nucleotides is not accompanied by scaffolding.

Cardiolipin Stimulates Lipid Tube Formation Induced by Drp1—Next we investigated the lipid dependence on Drp1 membrane activity. It has been reported previously that Drp1 shows a preferential binding to vesicles containing the specific mitochondrial lipid cardiolipin (30, 49, 50). This CL effect could be due to a specific recognition of the CL structure, to electrochemical interactions favored by the negative charge of this lipid, or to the negative intrinsic curvature induced in the membrane by CL. Strikingly, we found that replacing CL in the MLL mix with PC, which is a neutral lipid, completely abolished the ability of Drp1 to bind to these vesicles or to induce membrane remodeling (Fig. 2*C*). MLL-PC vesicles still contain a significant amount of negatively charged lipids, which suggests that additional features of CL besides its negative charge are required for Drp1 binding to membranes.

To test whether Drp1 binding is influenced by the intrinsic curvature of lipids, CL was substituted by phosphatidylglycerol (PG) or phosphatidic acid (PA) while maintaining the net charge of the vesicles. PG has a less negative intrinsic monolayer curvature than CL, whereas PA has more (51). In the case of PG-containing GUVs, Drp1-Al488 was capable of binding to the membrane (Fig. 2*C*), although with a distinct binding pattern from that observed in CL-containing vesicles. Drp1-Al488 did not cover the whole membrane surface and showed a patch-

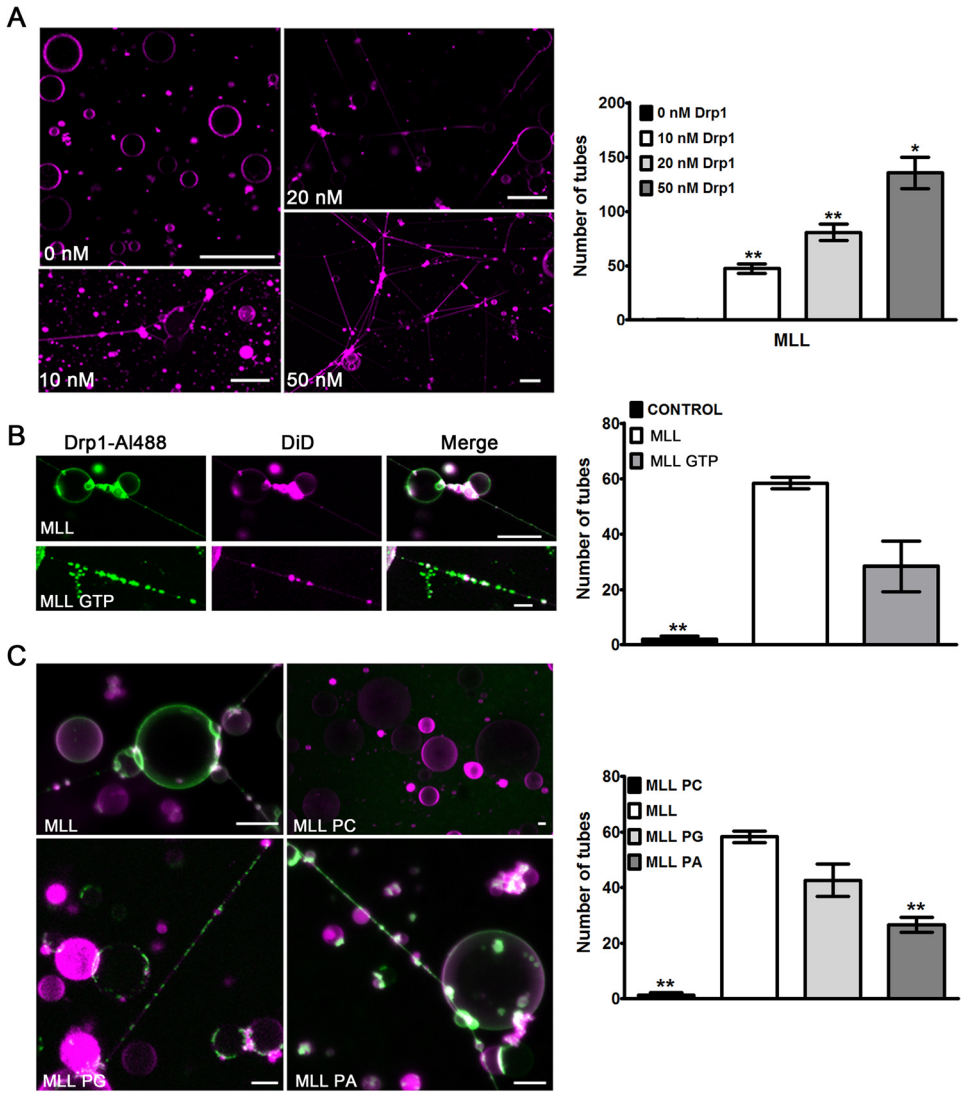

FIGURE 2. **Tube formation induced by Drp1 in GUVs.** *A–C*, confocal microscopy images (*right panels*) and tube quantification (*left panels*) of DiD-labeled MLL GUVs incubated in the absence or presence of unlabeled Drp1 (*A*); DiD-labeled MLL GUVs incubated with 25 nM Drp1-Al488 in the absence or presence of 1 mM GTP (*B*); DiD-labeled MLL, MLL PC, MLL PG, or MLL PA GUVs incubated with 25 nM Drp1-Al488 in the absence of GTP (*C*). *Scale bars* = 50 μm (*A*) and 10 μm (*B–C*). Data are mean ± S.D. of three independent experiments. *, $p < 0.05$; **, $p < 0.01$ *versus* MLL sample.

like binding pattern to MLL-PG GUVs, which suggests that CL is required for optimal binding of Drp1 to membranes (Fig. 2*C*). In contrast, when incubated with MLL-PA GUVs, Drp1-Al488 showed a similar binding pattern compared with CL-containing vesicles (Fig. 2*C*), and it bound homogeneously to the vesicle surfaces and tubes. When we quantified the number of tubes produced in GUV samples of the different lipid compositions, we found that Drp1-Al488 produced more lipid tubes in CL-containing vesicles compared with PA-containing ones, suggesting that Drp1-induced membrane tubulation is not exclusively mediated by the negative curvature of the lipid (Fig. 2*C*). Together, these results suggest that the specific structure of CL plays a role in Drp1-induced membrane tubulation, which can be at least partially substituted by PG.

GTP Promotes a Compact Assembly of Drp1 Related to Scaffolding—From the literature currently available, it remains unclear what role GTP plays in Drp1 binding to membranes and whether Drp1 oligomerization in solution is necessary for the nucleation of Drp1 higher order structures on membranes (22, 52). The results obtained so far indicate that Drp1 binding to membranes and tube formation are independent of GTP. To study the effect of GTP on membrane binding and remodeling of Drp1, we performed similar experiments as described above but in the presence of 1 mM GTP. Under these conditions, Drp1-induced membrane tubulation was also observed (Fig. 2*B*), although to a lesser extent.

The most striking finding, however, was that the binding pattern of Drp1-Al488 changed drastically in the presence of GTP. In particular, in the presence of GTP, membranes were completely covered by Drp1, together with the appearance of discrete Drp1-Al488 clusters or higher order oligomers on the surface of the vesicles (Fig. 3*A*). In addition, Drp1 was heterogeneously distributed on the tube surfaces and also appeared as segregated protein clusters along them (Fig. 2*B*). Drp1 clusters also appeared in solution, mostly associated with small lipid vesicles and/or aggregates. To confirm that the Drp1 clusters induced by GTP specifically bound to the membrane surface of MLL GUVs and were not an artifact because of random cluster

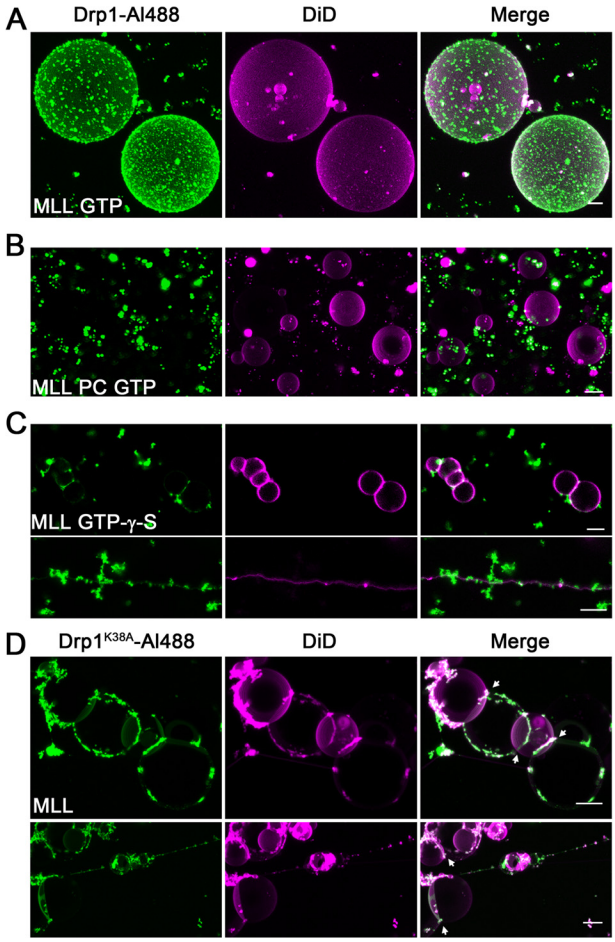

FIGURE 3. **GTP promotes Drp1 clustering in solution and in MLL GUVs.** Confocal microscopy images of DiD-labeled MLL GUVs incubated with Drp1-Al488 (25 nM) in the presence of 1 mM GTP (*A*); DiD-labeled MLL PC GUVs incubated with Drp1-Al488 (25 nM) in the presence of 1 mM GTP (*B*); DiD-labeled MLL GUVs incubated with Drp1-Al488 (25 nM) in the presence of 1 mM GTP-γ-S (*C*); and DiD-labeled MLL GUVs incubated with $Drp1^{K38A}$-Al488 (500 nM) in the absence of 1 mM GTP (*D*). *Scale bars* = 10 μm.

sedimentation, we checked that they did not appear on the membrane but remained in solution when the protein was incubated with MLL PC GUVs (Fig. 3*B*).

Drp1 binding to MLL GUVs was also observed in the presence of GTP-γ-S, a non-hydrolyzable GTP analog. As expected, Drp1 formed large clusters, which were visualized both in suspension and bound to the surface of vesicles and tubes (Fig. 3*C*). This indicates that Drp1 scaffolding on the membrane surface depends on GTP binding but not on its hydrolysis. Furthermore, the clusters observed in the presence of GTP-γ-S were larger than with GTP, suggesting that GTP hydrolysis leads to smaller oligomeric polymers.

As an additional control for GTP effects on Drp1 activity, we used a fluorescently labeled version of the dominant negative mutant $Drp1^{K38A}$ ($Drp1^{K38A}$-Al488). This dominant-negative mutation in Drp1 changes the critical lysine in the consensus G_1 motif to the GTPase domain into an alanine, presumably inhibiting GTP binding by Drp1 (9, 30, 35, 53). To compensate for the high tendency of this protein to aggregate (larger oligomers were already detected for purified $Drp1^{K38A}$-Al488, data not shown) (35), a higher concentration of the mutant protein was used in the experiments. In agreement with our previous observations, this Drp1 mutant was also capable of binding to membranes and inducing membrane remodeling (Fig. 3*D*). Interestingly, we observed a different binding pattern compared with wild-type Drp1, characterized by more protein aggregates and lipid-containing clusters attached to the GUVs.

Drp1 Induces Membrane Tethering and Concentrates at the Membrane Contact Surfaces—Surprisingly, we found that, in parallel to tube formation, Drp1 induced membrane tethering in adjacent GUVs in the absence of nucleotides (Fig. 4). The extent of vesicle tethering was as prominent as the formation of lipid tubes, suggesting that this is an important aspect of Drp1 membrane activity. In agreement with this, previous studies postulated the role of Drp1 in the formation of hemifusion/fission intermediates by detecting the aggregation of LUVs induced by Drp1 (30). Nevertheless, neither the specific structural rearrangements involved nor its implications for the role of Drp1 in membrane division have been addressed so far. Therefore, we decided to reevaluate the membrane-tethering activity of Drp1 in our GUV system.

The areas of tethered membranes induced by Drp1 were heterogeneous but normally spanned several square micrometers, in the order of the sizes of the giant vesicles (Fig. 4*A*, *white arrows*). Usually, pairs of vesicles appeared tethered, but it was not uncommon to observe larger structures with several GUVs attached to each other. Interestingly, the fluorescence intensity of Drp1-Al488 was higher on the contact sites than on the rest of the vesicle surface, indicating that the protein is concentrated at the tethered surfaces between adjacent vesicles (Fig. 4*A*). This preferential partitioning supports a direct role of the protein in the stabilization of these structures.

In addition, the membrane-tethering activity of Drp1-Al488 was increased in the presence of GTP, suggesting that this nucleotide could favor the process (Fig. 4*B*). However, the preferential partitioning of Drp1 to the membrane contact surfaces in tethered vesicles was less evident (Fig. 4*A*), which could be due to the overall increased membrane binding induced by GTP. Drp1-Al488 also induced membrane tethering in MLL PG and MLL PA GUVs and concentrated at the contact surfaces between adjacent vesicles (Fig. 4*A*). Interestingly, quantification of Drp1-induced membrane tethering suggested a role for the intrinsic negative curvature of lipids in this process because tethering increased in the following order: MLL PA > MLL ≥ MLL PG (Fig. 4*B*).

Quantitative Analysis of GTP and Lipid Composition Effects on the Membrane Activity of Drp1 by Flow Cytometry—Although allowing direct visualization and low number quantification of membrane binding and remodeling events, it is difficult to obtain statistically relevant quantitative information about these processes from imaging experiments with GUVs. In contrast, flow cytometry is a powerful technique that allows the simultaneous quantification of a number of parameters important for membrane activity for tens of thousands of events. These include total protein binding to a liposome population (quantified as geometric mean of fluorescence intensity), protein density on the membrane surface (calculated as corrected fluorescence units), and vesicle shape alterations like tethering (shape index) (40). To study the binding and tethering

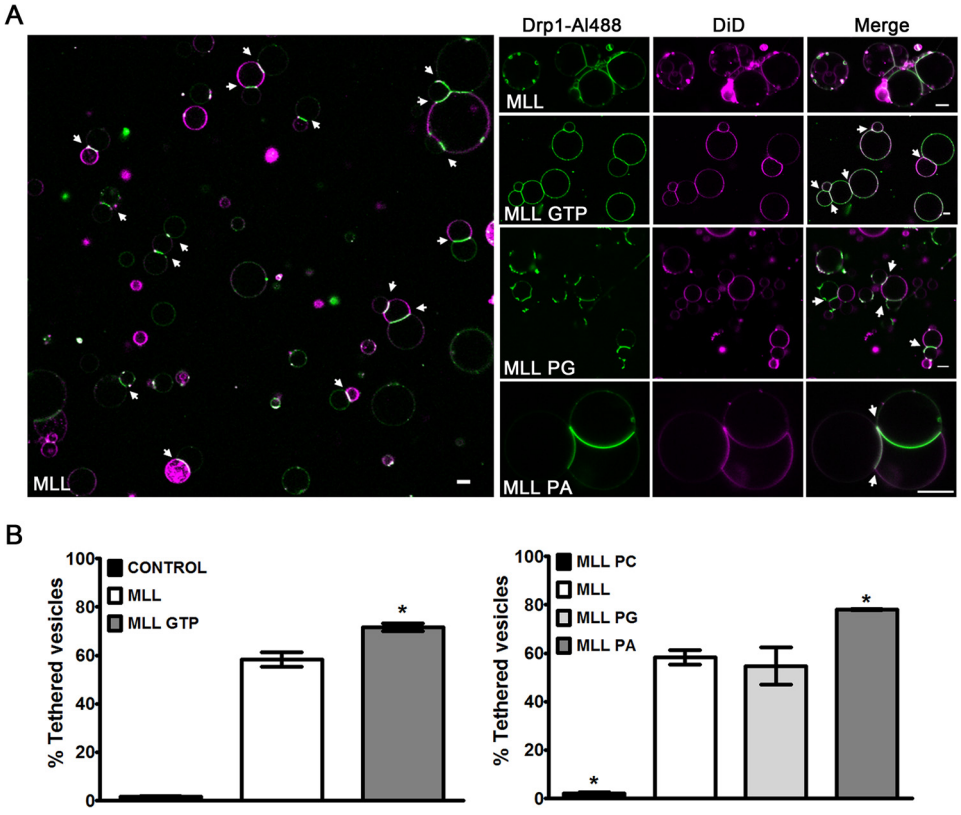

FIGURE 4. **Membrane tethering induced by Drp1 in GUVs.** *A* and *B*, confocal microscopy images (*A*) and quantification of tethered vesicles (*B*) of DiD-labeled MLL, MLL PG, and MLL PA GUVs incubated in the presence of Drp1-Al488 (25 nM). *Scale bars* = 10 μm. *Arrows* stand for the Drp1 localization in contact surfaces between adjacent vesicles. Data are mean ± S.D. of three independent experiments. *, $p < 0.05$; **, $p < 0.01$ *versus* MLL sample.

activity of Drp1 on liposomes by flow cytometry, Drp1-Al488 and 1% RhodPE-labeled LUVs were used. Rhod-PE-labeled liposomes were easily detected and gated on the basis of the rhodamine-derived fluorescence from the vesicles (Fig. 5*A*).

As mentioned above, Drp1 self-assembly is stimulated in the presence of GTP. To quantitatively analyze whether Drp1 binding to liposomes is influenced by the presence of GTP, we measured Drp1-Al488 binding to MLL LUVs in the absence or presence of GTP or GTP-γ-S. In agreement with the observations in GUVs, Drp1 showed a significantly greater binding to MLL LUVs in the presence of GTP. As expected, Drp1 membrane density was also enhanced in the presence of GTP, implying that Drp1 binds more efficiently to the membrane when nucleotides are present in the assay (Fig. 5*B*, *center panel*). However, binding in the presence of GTP-γ-S was not significantly different from binding in the absence of nucleotides (Fig. 5*B*, *top panel*), suggesting that the larger Drp1 oligomers bind less to membranes.

To quantitatively analyze the role of CL on Drp1 binding to liposomes, we used a number of MLL LUVs deficient in CL, where this lipid was substituted by PC, PS, PG, or PA. In the case of negatively charged lipids (*i.e.* PS, PG, and PA), the net charge of the vesicles was maintained (see "Experimental Procedures"). We found that Drp1 binding to membranes was directly linked to the negative intrinsic monolayer curvature of the selected lipid. According to this, binding was most efficient in the presence of PA and increased in the following order: MLL PC (not detectable) << MLL PG < MLL PS < MLL < MLL PA (Fig. 5*C*, *top panel*). We then studied Drp1 membrane density, taking into account Drp1-induced liposome size variations. In this case, Drp1 showed similar binding density independent of the lipid composition tested, except for MLL PC LUVs, where no detectable interaction was found (Fig. 5*C*, *center panel*).

Furthermore, we analyzed the membrane shape alterations induced by Drp1. GTP, but not by GTP-γ-S, promoted Drp1-induced membrane tethering when compared with the shape index in the absence of nucleotide (Fig. 5*B*, *bottom panel*). Interestingly, this result suggests that larger Drp1 oligomers have less potential to induce membrane tethering. Moreover, when CL was replaced by different negatively charged lipids, Drp1 induced variations in liposome size (*i.e.* membrane tethering). This was again tightly dependent on the negative intrinsic monolayer curvature of the substituted lipid, increasing in the following order: MLL PC (no detectable size variation) << MLL PG < MLL PS < MLL < MLL PA (Fig. 5*C*, *bottom panel*). Overall, these results are in agreement with and provide a sound statistical support for the results obtained with GUVs.

Tethered Mitochondria Are Observed during the Last Steps of Drp1-induced Division in Cells—It is important to note that tethered membranes similar to those found in GUVs also seem to be present during Drp1-mediated mitochondrial division. Indeed, previous studies with GFP-tagged Drp1 have reported that Drp1 fission complexes remain associated with both ends of divided mitochondria (34). Similar observations have been made for Dnm1 in yeast (13). This implies that, prior to the separation of the two daughter mitochondria and after mem-

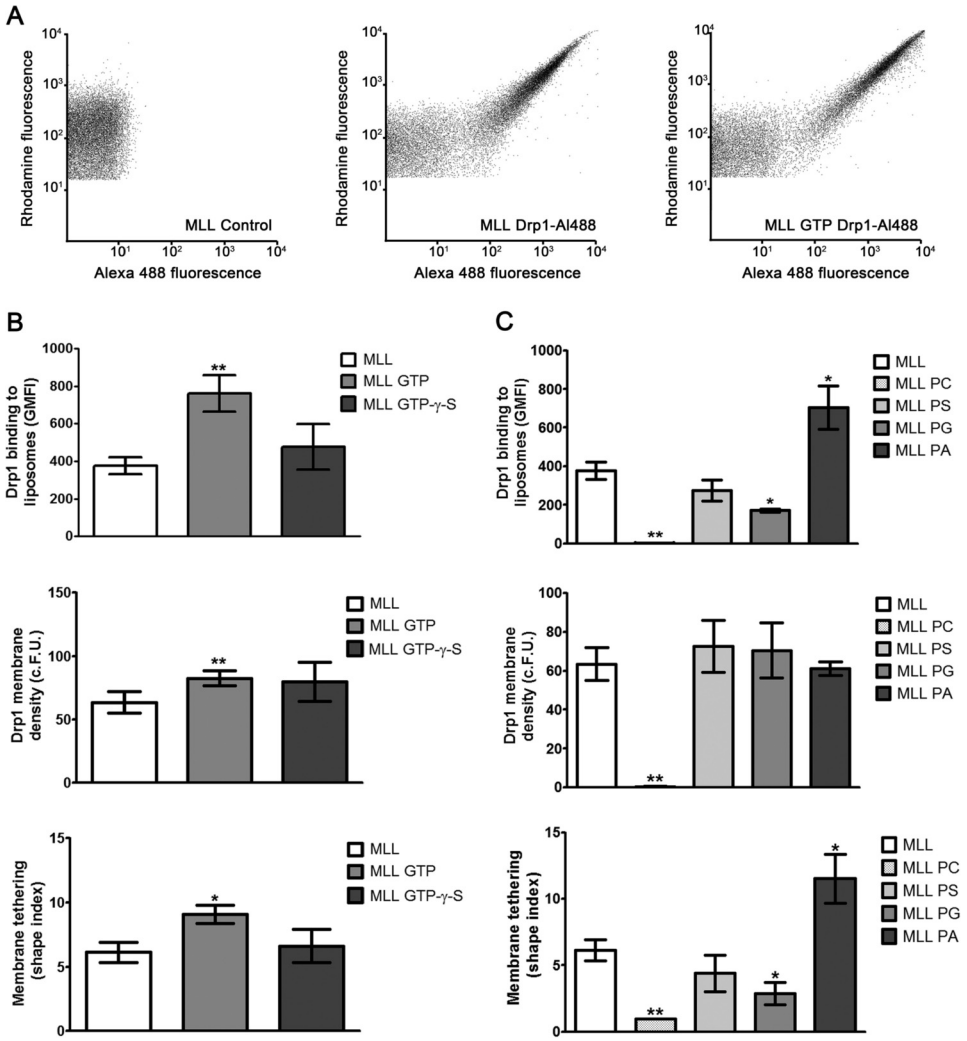

FIGURE 5. **Analysis of Drp1-liposome interactions and Drp1-induced liposome shape alterations by flow cytometry.** *A*, representative flow cytometry plots outlining Drp1 binding to MLL LUVs in the absence or presence of GTP. *B* and *C*, Drp1 binding to a liposome population (geometric mean of fluorescence intensity, *GMFI*, *top panels*), Drp1 membrane density (c.F.U.: corrected fluorescence units, *c.F.U.*, *center panels*), and Drp1-induced membrane tethering (*bottom panels*) in MLL LUVs in the absence or presence of GTP and GTP-γ-S (*B*) and in MLL, MLL PC, MLL PS, MLL PG, and MLL PA LUVs in the absence of nucleotides (*C*). Drp1 binding per normalized liposome and membrane tethering were described previously (40). Shape index values (*y* axis) above 1 are indicative of an increase (negative membrane curvature or tethering) in a rhodamine-derived signal averaged for all liposome size gates. Data are mean ± S.D. of four independent experiments. *, $p < 0.05$; **, $p < 0.01$ *versus* MLL sample.

brane fission has taken place, the two newly generated membranes remain transiently apposed. Following this, final separation is achieved by migration of the daughter mitochondria as they are pulled by the cytoskeleton. To confirm that tethered daughter mitochondria are found in cells, we analyzed the steps involved in mitochondrial division by live microscopy in mouse embryonic fibroblast cells transiently transfected with GFP-Drp1. Despite the difficulties to capture these events, Fig. 6*A* shows a representative example of tethered mitochondria where Drp1 was localized at contact sites between both mitochondrial parts. Importantly, this happened after recruitment of Drp1 into discrete foci at the mitochondrial surface and membrane scission but before separation of the daughter mitochondria. Later on, mitochondrial fission proceeded with both mitochondrial tails separating and carrying Drp1 complexes attached to the new mitochondrial poles. This suggests that the break point in mitochondrial division is at the middle of the Drp1 filament, in contrast to the model proposed by Roux and colleagues (54, 55) for dynamin. In addition, these results are supported by immunostaining of endogenous Drp1 in cells containing mitochondria labeled with Mito-DsRed, where three types of Drp1 structures related to mitochondrial division can be distinguished (Fig. 6*B*): Drp1 bound to mitochondria in a constricted state; Drp1 bound to mitochondria that have been divided but that remain in a tethered state; and Drp1 bound at mitochondrial ends, likely the final product of mitochondrial division. The large number of events showing divided mitochondria in a tethered conformation (16.3% ± 4.9 from $n = 1541$ structures analyzed, 10 cells) supports the biological relevance of this structure.

DISCUSSION

Here we characterized the membrane activity of Drp1 using chemically controlled reconstituted systems that mimic physiological conditions. We investigated the membrane binding and remodeling properties of Drp1, including membrane tubu-

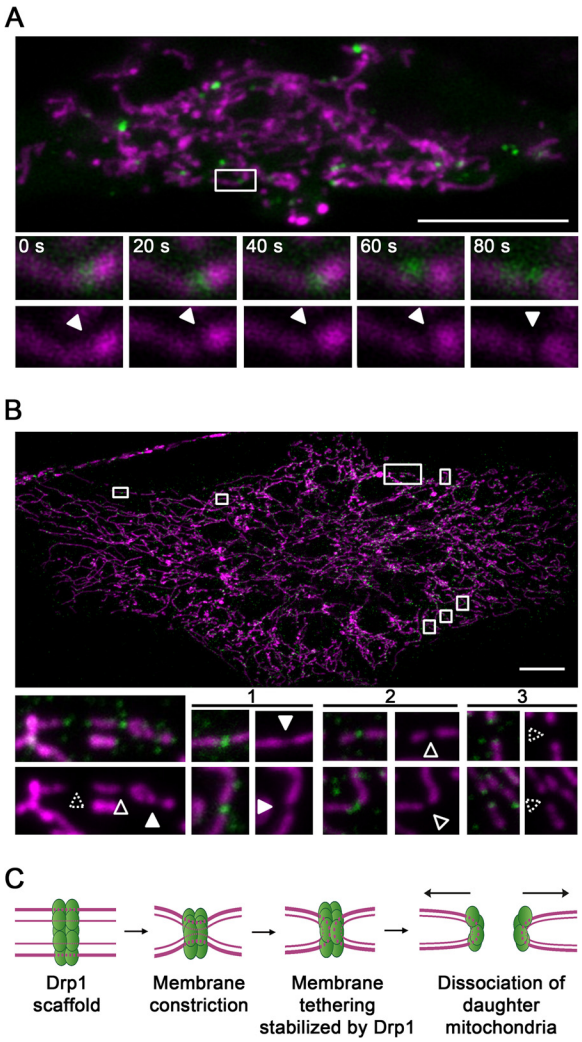

FIGURE 6. **Drp1-induced mitochondrial division in mammalian cells.** *A*, confocal microscopy images of Drp1-induced mitochondrial division in living mouse embryonic fibroblast cells. Overview (*top panel*) and zoom images (*bottom panels*) of a fission event. *Arrowheads* indicate the positions of GFP-Drp1 in the mitochondrial fission process. *Green*, Drp1; *magenta*, mitochondria. *Scale bar* = 10 μm. *B*, confocal microscopy image of endogenous Drp1 located at the mitochondria of one representative HeLa cell. The areas in the *white squares* are shown enlarged below, where zoom images show three different structures in mitochondria where Drp1 is localized. *1*, constricted membranes (*filled arrowheads*) (63.7% $\pm$ 9.2); *2*, tethered membranes (*open arrowheads*) (16.3% $\pm$ 4.9); *3*, dissociated membranes (*dashed arrowheads*) (20.6% $\pm$ 7.1), (n = 1541 structures analyzed, 10 cells). *Green*, Drp1; *magenta*, mitochondria. *Scale bar* = 10 μm. *C*, model proposed for Drp1-induced mitochondrial fission. Only the outer mitochondrial membrane is shown, where the *thick line* represents the outer leaflet and the *thin line* represents the inner leaflet.

lation and tethering, and examined the role of lipids and of GTP on these processes. As discussed below, the results reported here may be relevant for the molecular mechanism of action of Drp1 in the cellular context.

Fluorescent labeling of Drp1 allowed us not only to specifically locate Drp1 on the vesicles but also to study the lipid determinants for Dpr1 membrane binding. We show that Drp1 binding to vesicles mimicking the lipid composition of the mitochondrial outer membrane (MLL GUVs) requires CL or a negatively charged lipid with negative intrinsic curvature (like PA). Only 4.35% CL, a concentration typically found on the mitochondrial outer membrane, was sufficient to induce Drp1 binding to GUVs. Fully replacing CL with PC abrogated Drp1 binding. Exchanging CL with other negatively charged lipids like PG or PA also led to Drp1 association to GUVs, although it affected the binding pattern. Taken together, these results suggest that maintaining the net negative charge of the vesicles is not the only parameter affecting Drp1 membrane binding but that the intrinsic monolayer curvature of the lipids also plays a role. Therefore, and contrary to what is believed in the field (49, 50), our results show that CL is not essential for Drp1 binding to membranes. Indeed, Drp1 also catalyzes peroxisomal division (10, 56), suggesting that a common mechanism exists for mitochondrial and peroxisomal division. However, peroxisomal CL content is thought to be negligible (57, 58). Interestingly, PA is enriched in maturated peroxisomes (59). In this context, our results reinforce the view that PA could play a role for Drp1 recruitment to peroxisomal membranes.

In cells, Drp1 bound to mitochondria is not homogeneously distributed. Instead, it concentrates at discrete foci (9, 60), which is thought to be mediated by specific binding to adaptor proteins (17, 18, 21, 31). Recent evidence suggests that these Drp1 foci are structurally distinct platforms for a number of mitochondrion-related processes, characterized by a concrete protein and lipid composition (61–65). On the basis of our results, it is therefore tempting to speculate that enrichment of CL or other negatively charged lipids with negative intrinsic curvature might also play a role in regulating Drp1 segregation to these foci.

Moreover, we also found that, in contrast to what has been observed for other members of the dynamin family (48, 66, 67), Drp1 bound to both flat and curved membranes in the absence of nucleotides. This is unexpected because curvature sensing is believed to be a key property of dynamin proteins, and it suggests a fundamentally different mechanism of action for Drp1. Indeed, in cells, dynamin binding to endocytic vesicles happens only before the final event of membrane fission (68–70). Instead, Drp1 is continuously shuttling between the cytosol and mitochondria, and only a fraction of the foci containing bound Drp1 develop into mitochondrial division sites (9). Furthermore, we show that GTP induced a compact assembly of Drp1 on the membrane surface, in contrast to the homogeneous distribution of the protein on the GUVs in the absence of nucleotides. These clusters are also found on flat and curved membranes and are likely related to Drp1 scaffolding because GTP and GTP analogs have been shown to induce Drp1 oligomerization (29, 31, 49, 71). Therefore, our results reveal two distinct modes of curvature-independent Drp1 binding to membranes that set it apart from other members of the dynamin family and that may be relevant for the molecular mode of action of Drp1 in the context of the cell.

Previous studies have shown that Drp1 deforms liposomes into tubules using electron microscopy (26, 29, 31). However, this membrane tubulation activity has remained under debate because it was observed under experimental conditions far from those found in mitochondria, including non-biologically relevant lipid compositions and protein concentrations as well as harsh sample treatments (26, 31). Here we show that Drp1 promotes membrane tubulation when incubated with GUVs mimicking the lipid composition of mitochondria at low con-

centrations and at room temperature. In addition, tube formation seems to be independent of GTP and affected by the lipid composition of the membrane, with CL acting as a stimulator of this activity. These results indicate that, although Drp1 does not sense membrane curvature, it can stabilize lipid tubes and suggest that at least one of the functions of Drp1 in mitochondrial division is to stabilize curved membranes. Importantly, this activity can be separated from its proposed role in membrane constriction, which is thought to be linked to GTP hydrolysis.

Moreover, we report that Drp1 promotes vesicle tethering by inducing close contacts between large surfaces of the two apposed membranes. The extent of this membrane-tethering activity is similar to that of tube formation, indicating that this is also an important aspect of Drp1 action on membranes. Although they may not represent the same process, our data are in line with previous work performed by Montessuit *et al.* (30), where unlabeled Drp1 induced liposome aggregation and membrane hemifusion depending on the presence of ATP. Indeed, we detected membrane tethering in the absence of nucleotides, suggesting that neither GTP nor ATP are required for this process. Nevertheless, the intrinsic negative curvature of the lipids correlated with Drp1 membrane-tethering activity (PA > CL > PG ≈ PS), suggesting that non-lamellar membrane fission intermediates seemed to be involved, as also observed for vesicle aggregation (30, 51, 72).

By directly visualizing the tethered membranes, we found that Drp1 concentrated at contact surfaces between adjacent vesicles, suggesting that Drp1 induces GUV tethering by linking two membrane surfaces. This is interesting because membrane fission as well as fusion are topologically equivalent. That is, they proceed along the same pathway of structural intermediates but in opposite directions (Fig. 6*C*). These intermediate structures involve non-lamellar lipid assemblies and necessarily finish (or start, in the case of membrane fusion) with a local connection between the contacting monolayers of the two newly formed membranes before they finally separate (73). The same way that membrane tethering is an essential first step for fusing two membranes (for example by SNARE proteins), it is also the last step for membrane division. The preferential localization of Drp1-Al488 at those contact sites strongly suggests that Drp1 plays a role in the stabilization of these membrane fission intermediates (74). If one thinks in terms of energy and kinetics of a reaction, Drp1, by stabilizing tethered membranes, is able to lower the energy of the reaction product of mitochondrial division (that is, two apposed membranes) and, therefore, promote the reaction in the fission direction. In agreement with this new concept, we show that, in cells, Drp1-mediated mitochondrial division proceeds via tethered mitochondrial structures comparable with those observed in GUVs. These intermediate states are observed after membrane scission and prior to the separation of the divided mitochondria mediated by opposed pulling forces likely exerted by the cytoskeleton. In agreement with this, membrane division at the middle point of the Drp1 filament has been reported previously in various publications (26, 34), although without any mechanistic connection.

Our results show that GTP is not essential for Drp1 binding to membranes nor for its membrane tube formation or tethering activity but, rather, that it plays a role in the scaffolding of Drp1 molecules on the membrane surface, which may also increase the affinity for the membrane. The higher order structures visualized with GTP-γ-S suggest that GTP hydrolysis would lead to the disassembly, at least in part, of these oligomers, therefore limiting their growth. This is in agreement with previous studies (29, 31, 33) and with the finding that the extent of Drp1-mediated membrane remodeling anticorrelated with Drp1 oligomerization propensity in solution (50). Together, this suggests that Drp1 binding to GTP causes concentric assembly of Drp1 and that, upon GTP hydrolysis, Drp1 dissociates to smaller subunit forms. Moreover, these GTP-induced Drp1 clusters were also present along the tubes with a similar distribution pattern as dynamin (48, 54), suggesting that those sites could represent potential nucleation points for mitochondrial fission. Along these lines, previous work reported that long dynamin scaffolds did not produce membrane scission, whereas GTPase-dependent cycles of assembly and stochastic disassembly of short dynamin scaffolds led to fission (66, 75).

It is important to note that we were not able to visualize any fission event under the experimental conditions tested. Indeed, the fact that the membrane fission activity of Drp1 has not yet been reconstituted *in vitro* suggests, together with the large diameter found for Drp1 tubules in electron microscopy studies (26, 31, 50), that additional catalysis steps beyond membrane constriction and/or components are required to overcome the high-energy barrier of membrane fission so that Drp1 can mediate mitochondrial division. Taking this into account and on the basis of our findings and the data in the literature, we propose a new model for Drp1-induced mitochondrial fission (Fig. 6*C*). According to this model, besides Drp1-induced constriction of the mitochondrial tubular structure and the probable role of additional factors in further constricting mitochondria, Drp1 would also contribute to mitochondrial fission by stabilizing structural intermediates formed during the process by stabilizing the tethered new mitochondrial poles before their dissociation.

In summary, we report direct visualization of Drp1 binding to membranes and membrane remodeling activity under conditions mimicking the mitochondrial environment. We demonstrate that Drp1 binds to both curved and flat membranes independently of GTP and that GTP promotes Drp1 clustering on the membrane surface. Moreover, we show that Drp1 induces lipid tubes as well as membrane fission intermediates affected by the presence of lipids with a negative intrinsic monolayer curvature. Our results support a mechanism by which Drp1, besides its function in membrane constriction, plays a role on the stabilization of the structural intermediates involved in the final step of membrane fission.

Acknowledgments—We thank Carolin Stegmüller and Britta Liebler for technical support, Joseph Unsay for model design, Raquel Salvador Gallego and Aida Peña Blanco for helpful advice with cell experiments, Dr. C. Blackstone for the pCal-n-EK-Drp1 and pCal-n-EK-Drp1^{K38A} constructs, and Dr. M. Jendrach for the pEGFP-C1-Drp1 plasmid.

REFERENCES

1. Osman, C., Voelker, D. R., and Langer, T. (2011) Making heads or tails of phospholipids in mitochondria. *J. Cell Biol.* **192,** 7–16
2. Glancy, B., and Balaban, R. S. (2012) Role of mitochondrial Ca^{2+} in the regulation of cellular energetics. *Biochemistry* **51,** 2959–2973
3. Chan, D. C. (2012) Fusion and fission: interlinked processes critical for mitochondrial health. *Annu. Rev. Genet.* **46,** 265–287
4. Okamoto, K., and Shaw, J. M. (2005) Mitochondrial morphology and dynamics in yeast and multicellular eukaryotes. *Annu. Rev. Genet.* **39,** 503–536
5. Youle, R. J., and van der Bliek, A. M. (2012) Mitochondrial fission, fusion, and stress. *Science* **337,** 1062–1065
6. Friedman, J. R., and Nunnari, J. (2014) Mitochondrial form and function. *Nature* **505,** 335–343
7. van den Bosch, H., Schutgens, R. B., Wanders, R. J., and Tager, J. M. (1992) Biochemistry of peroxisomes. *Annu. Rev. Biochem.* **61,** 157–197
8. Itoyama, A., Michiyuki, S., Honsho, M., Yamamoto, T., Moser, A., Yoshida, Y., and Fujiki, Y. (2013) Mff functions with Pex11pβ and DLP1 in peroxisomal fission. *Biol. Open* **2,** 998–1006
9. Smirnova, E., Griparic, L., Shurland, D. L., and van der Bliek, A. M. (2001) Dynamin-related protein Drp1 is required for mitochondrial division in mammalian cells. *Mol. Biol. Cell* **12,** 2245–2256
10. Li, X., and Gould, S. J. (2003) The dynamin-like GTPase DLP1 is essential for peroxisome division and is recruited to peroxisomes in part by PEX11. *J. Biol. Chem.* **278,** 17012–17020
11. Mozdy, A. D., McCaffery, J. M., and Shaw, J. M. (2000) Dnm1p GTPase-mediated mitochondrial fission is a multi-step process requiring the novel integral membrane component Fis1p. *J. Cell Biol.* **151,** 367–380
12. Tieu, Q., and Nunnari, J. (2000) Mdv1p is a WD repeat protein that interacts with the dynamin-related GTPase, Dnm1p, to trigger mitochondrial division. *J. Cell Biol.* **151,** 353–366
13. Naylor, K., Ingerman, E., Okreglak, V., Marino, M., Hinshaw, J. E., and Nunnari, J. (2006) Mdv1 interacts with assembled dnm1 to promote mitochondrial division. *J. Biol. Chem.* **281,** 2177–2183
14. Lackner, L. L., Horner, J. S., and Nunnari, J. (2009) Mechanistic analysis of a dynamin effector. *Science* **325,** 874–877
15. Koch, A., Yoon, Y., Bonekamp, N. A., McNiven, M. A., and Schrader, M. (2005) A role for Fis1 in both mitochondrial and peroxisomal fission in mammalian cells. *Mol. Biol. cell* **16,** 5077–5086
16. Gandre-Babbe, S., and van der Bliek, A. M. (2008) The novel tail-anchored membrane protein Mff controls mitochondrial and peroxisomal fission in mammalian cells. *Mol. Biol. Cell* **19,** 2402–2412
17. Otera, H., Wang, C., Cleland, M. M., Setoguchi, K., Yokota, S., Youle, R. J., and Mihara, K. (2010) Mff is an essential factor for mitochondrial recruitment of Drp1 during mitochondrial fission in mammalian cells. *J. Cell Biol.* **191,** 1141–1158
18. Palmer, C. S., Osellame, L. D., Laine, D., Koutsopoulos, O. S., Frazier, A. E., and Ryan, M. T. (2011) MiD49 and MiD51, new components of the mitochondrial fission machinery. *EMBO Rep.* **12,** 565–573
19. Zhao, J., Liu, T., Jin, S., Wang, X., Qu, M., Uhlén, P., Tomilin, N., Shupliakov, O., Lendahl, U., and Nistér, M. (2011) Human MIEF1 recruits Drp1 to mitochondrial outer membranes and promotes mitochondrial fusion rather than fission. *EMBO J.* **30,** 2762–2778
20. Palmer, C. S., Elgass, K. D., Parton, R. G., Osellame, L. D., Stojanovski, D., and Ryan, M. T. (2013) Adaptor proteins MiD49 and MiD51 can act independently of Mff and Fis1 in Drp1 recruitment and are specific for mitochondrial fission. *J. Biol. Chem.* **288,** 27584–27593
21. Losón, O. C., Song, Z., Chen, H., and Chan, D. C. (2013) Fis1, Mff, MiD49, and MiD51 mediate Drp1 recruitment in mitochondrial fission. *Mol. Biol. Cell* **24,** 659–667
22. Ingerman, E., Perkins, E. M., Marino, M., Mears, J. A., McCaffery, J. M., Hinshaw, J. E., and Nunnari, J. (2005) Dnm1 forms spirals that are structurally tailored to fit mitochondria. *J. Cell Biol.* **170,** 1021–1027
23. Mears, J. A., Lackner, L. L., Fang, S., Ingerman, E., Nunnari, J., and Hinshaw, J. E. (2011) Conformational changes in Dnm1 support a contractile mechanism for mitochondrial fission. *Nat. Struct. Mol. Biol.* **18,** 20–26
24. Faelber, K., Posor, Y., Gao, S., Held, M., Roske, Y., Schulze, D., Haucke, V., Noé, F., and Daumke, O. (2011) Crystal structure of nucleotide-free dynamin. *Nature* **477,** 556–560
25. Ford, M. G., Jenni, S., and Nunnari, J. (2011) The crystal structure of dynamin. *Nature* **477,** 561–566
26. Fröhlich, C., Grabiger, S., Schwefel, D., Faelber, K., Rosenbaum, E., Mears, J., Rocks, O., and Daumke, O. (2013) Structural insights into oligomerization and mitochondrial remodelling of dynamin 1-like protein. *EMBO J.* **32,** 1280–1292
27. Chappie, J. S., Acharya, S., Leonard, M., Schmid, S. L., and Dyda, F. (2010) G domain dimerization controls dynamin's assembly-stimulated GTPase activity. *Nature* **465,** 435–440
28. Chappie, J. S., Mears, J. A., Fang, S., Leonard, M., Schmid, S. L., Milligan, R. A., Hinshaw, J. E., and Dyda, F. (2011) A pseudoatomic model of the dynamin polymer identifies a hydrolysis-dependent powerstroke. *Cell* **147,** 209–222
29. Yoon, Y., Pitts, K. R., and McNiven, M. A. (2001) Mammalian dynamin-like protein DLP1 tubulates membranes. *Mol. Biol. Cell* **12,** 2894–2905
30. Montessuit, S., Somasekharan, S. P., Terrones, O., Lucken-Ardjomande, S., Herzig, S., Schwarzenbacher, R., Manstein, D. J., Bossy-Wetzel, E., Basañez, G., Meda, P., and Martinou, J. C. (2010) Membrane remodeling induced by the dynamin-related protein Drp1 stimulates Bax oligomerization. *Cell* **142,** 889–901
31. Koirala, S., Guo, Q., Kalia, R., Bui, H. T., Eckert, D. M., Frost, A., and Shaw, J. M. (2013) Interchangeable adaptors regulate mitochondrial dynamin assembly for membrane scission. *Proc. Natl. Acad. Sci. U.S.A.* **110,** E1342–E1351
32. Wenger, J., Klinglmayr, E., Frohlich, C., Eibl, C., Gimeno, A., Hessenberger, M., Puehringer, S., Daumke, O., and Goettig, P. (2013) Functional mapping of human dynamin-1-like GTPase domain based on x-ray structure analyses. *PLoS ONE* **8,** e71835
33. Losón, O. C., Liu, R., Rome, M. E., Meng, S., Kaiser, J. T., Shan, S. O., and Chan, D. C. (2014) The mitochondrial fission receptor MiD51 requires ADP as a cofactor. *Structure* **22,** 367–377
34. Strack, S., and Cribbs, J. T. (2012) Allosteric modulation of Drp1 mechanoenzyme assembly and mitochondrial fission by the variable domain. *J. Biol. Chem.* **287,** 10990–11001
35. Zhu, P. P., Patterson, A., Stadler, J., Seeburg, D. P., Sheng, M., and Blackstone, C. (2004) Intra- and intermolecular domain interactions of the C-terminal GTPase effector domain of the multimeric dynamin-like GTPase Drp1. *J. Biol. Chem.* **279,** 35967–35974
36. Chang, C. R., Manlandro, C. M., Arnoult, D., Stadler, J., Posey, A. E., Hill, R. B., and Blackstone, C. (2010) A lethal *de novo* mutation in the middle domain of the dynamin-related GTPase Drp1 impairs higher order assembly and mitochondrial division. *J. Biol. Chem.* **285,** 32494–32503
37. Leonard, M., Song, B. D., Ramachandran, R., and Schmid, S. L. (2005) Robust colorimetric assays for dynamin's basal and stimulated GTPase activities. *Methods Enzymol.* **404,** 490–503
38. García-Sáez, A. J., Ries, J., Orzáez, M., Pérez-Payà, E., and Schwille, P. (2009) Membrane promotes tBID interaction with BCL(XL). *Nat. Struct. Mol. Biol.* **16,** 1178–1185
39. Bleicken, S., Garcia-Saez, A. J., Conte, E., and Bordignon, E. (2012) Dynamic interaction of cBid with detergents, liposomes and mitochondria. *PLoS ONE* **7,** e35910
40. Temmerman, K., and Nickel, W. (2009) A novel flow cytometric assay to quantify interactions between proteins and membrane lipids. *J. Lipid Res.* **50,** 1245–1254
41. Mai, S., Klinkenberg, M., Auburger, G., Bereiter-Hahn, J., and Jendrach, M. (2010) Decreased expression of Drp1 and Fis1 mediates mitochondrial elongation in senescent cells and enhances resistance to oxidative stress through PINK1. *J. Cell Sci.* **123,** 917–926
42. Sever, S., Muhlberg, A. B., and Schmid, S. L. (1999) Impairment of dynamin's GAP domain stimulates receptor-mediated endocytosis. *Nature* **398,** 481–486
43. Stowell, M. H., Marks, B., Wigge, P., and McMahon, H. T. (1999) Nucleotide-dependent conformational changes in dynamin: evidence for a mechanochemical molecular spring. *Nat. Cell Biol.* **1,** 27–32
44. Chen, Y. J., Zhang, P., Egelman, E. H., and Hinshaw, J. E. (2004) The stalk region of dynamin drives the constriction of dynamin tubes. *Nat. Struct.*

Mol. Biol. **11,** 574–575
45. Sever, S., Skoch, J., Newmyer, S., Ramachandran, R., Ko, D., McKee, M., Bouley, R., Ausiello, D., Hyman, B. T., and Bacskai, B. J. (2006) Physical and functional connection between auxilin and dynamin during endocytosis. *EMBO J.* **25,** 4163–4174
46. Ramachandran, R., Surka, M., Chappie, J. S., Fowler, D. M., Foss, T. R., Song, B. D., and Schmid, S. L. (2007) The dynamin middle domain is critical for tetramerization and higher-order self-assembly. *EMBO J.* **26,** 559–566
47. Horvath, S. E., and Daum, G. (2013) Lipids of mitochondria. *Prog. Lipid Res.* **52,** 590–614
48. Roux, A., Koster, G., Lenz, M., Sorre, B., Manneville, J. B., Nassoy, P., and Bassereau, P. (2010) Membrane curvature controls dynamin polymerization. *Proc. Natl. Acad. Sci. U.S.A.* **107,** 4141–4146
49. Bustillo-Zabalbeitia, I., Montessuit, S., Raemy, E., Basañez, G., Terrones, O., and Martinou, J.-C. (2014) Specific interaction with cardiolipin triggers functional activation of dynamin-related protein 1. *PloS ONE* **9,** e102738
50. Macdonald, P. J., Stepanyants, N., Mehrotra, N., Mears, J. A., Qi, X., Sesaki, H., and Ramachandran, R. (2014) A dimeric equilibrium intermediate nucleates Drp1 reassembly on mitochondrial membranes for fission. *Mol. Biol. cell* **25,** 1905–1915
51. Lewis, R. N., and McElhaney, R. N. (2000) Surface charge markedly attenuates the nonlamellar phase-forming propensities of lipid bilayer membranes: calorimetric and ^{31}P-nuclear magnetic resonance studies of mixtures of cationic, anionic, and zwitterionic lipids. *Biophys. J.* **79,** 1455–1464
52. Bhar, D., Karren, M. A., Babst, M., and Shaw, J. M. (2006) Dimeric Dnm1-G385D interacts with Mdv1 on mitochondria and can be stimulated to assemble into fission complexes containing Mdv1 and Fis1. *J. Biol. Chem.* **281,** 17312–17320
53. Smirnova, E., Shurland, D. L., Ryazantsev, S. N., and van der Bliek, A. M. (1998) A human dynamin-related protein controls the distribution of mitochondria. *J. Cell Biol.* **143,** 351–358
54. Morlot, S., Galli, V., Klein, M., Chiaruttini, N., Manzi, J., Humbert, F., Dinis, L., Lenz, M., Cappello, G., and Roux, A. (2012) Membrane shape at the edge of the dynamin helix sets location and duration of the fission reaction. *Cell* **151,** 619–629
55. Morlot, S., and Roux, A. (2013) Mechanics of dynamin-mediated membrane fission. *Annu. Rev. Biophys.* **42,** 629–649
56. Kobayashi, S., Tanaka, A., and Fujiki, Y. (2007) Fis1, DLP1, and Pex11p coordinately regulate peroxisome morphogenesis. *Exp. Cell Res.* **313,** 1675–1686
57. Schumann, U., and Subramani, S. (2008) Special delivery from mitochondria to peroxisomes. *Trends Cell Biol.* **18,** 253–256
58. Schrader, M., Bonekamp, N. A., and Islinger, M. (2012) Fission and proliferation of peroxisomes. *Biochim. Biophys. Acta* **1822,** 1343–1357
59. Guo, T., Gregg, C., Boukh-Viner, T., Kyryakov, P., Goldberg, A., Bourque, S., Banu, F., Haile, S., Milijevic, S., San, K. H., Solomon, J., Wong, V., and Titorenko, V. I. (2007) A signal from inside the peroxisome initiates its division by promoting the remodeling of the peroxisomal membrane. *J. Cell Biol.* **177,** 289–303
60. Labrousse, A. M., Zappaterra, M. D., Rube, D. A., and van der Bliek, A. M. (1999) *C. elegans* dynamin-related protein DRP-1 controls severing of the mitochondrial outer membrane. *Mol. Cell* **4,** 815–826
61. Karbowski, M., Lee, Y.-J., Gaume, B., Jeong, S.-Y., Frank, S., Nechushtan, A., Santel, A., Fuller, M., Smith, C. L., and Youle, R. J. (2002) Spatial and temporal association of Bax with mitochondrial fission sites, Drp1, and Mfn2 during apoptosis. *J. Cell Biol.* **159,** 931–938
62. Brooks, C., Wei, Q., Feng, L., Dong, G., Tao, Y., Mei, L., Xie, Z.-J., and Dong, Z. (2007) Bak regulates mitochondrial morphology and pathology during apoptosis by interacting with mitofusins. *Proc. Natl. Acad. Sci. U.S.A.* **104,** 11649–11654
63. Wasiak, S., Zunino, R., and McBride, H. M. (2007) Bax/Bak promote sumoylation of DRP1 and its stable association with mitochondria during apoptotic cell death. *J. Cell Biol.* **177,** 439–450
64. Suen, D. F., Norris, K. L., and Youle, R. J. (2008) Mitochondrial dynamics and apoptosis. *Genes Dev.* **22,** 1577–1590
65. Friedman, J. R., Lackner, L. L., West, M., DiBenedetto, J. R., Nunnari, J., and Voeltz, G. K. (2011) ER tubules mark sites of mitochondrial division. *Science* **334,** 358–362
66. Bashkirov, P. V., Akimov, S. A., Evseev, A. I., Schmid, S. L., Zimmerberg, J., and Frolov, V. A. (2008) GTPase cycle of dynamin is coupled to membrane squeeze and release, leading to spontaneous fission. *Cell* **135,** 1276–1286
67. Neumann, S., and Schmid, S. L. (2013) Dual role of BAR domain-containing proteins in regulating vesicle release catalyzed by the GTPase, dynamin-2. *J. Biol. Chem.* **288,** 25119–25128
68. Merrifield, C. J., Feldman, M. E., Wan, L., and Almers, W. (2002) Imaging actin and dynamin recruitment during invagination of single clathrin-coated pits. *Nat. Cell Biol.* **4,** 691–698
69. Ehrlich, M., Boll, W., Van Oijen, A., Hariharan, R., Chandran, K., Nibert, M. L., and Kirchhausen, T. (2004) Endocytosis by random initiation and stabilization of clathrin-coated pits. *Cell* **118,** 591–605
70. Rappoport, J. Z., Heyman, K. P., Kemal, S., and Simon, S. M. (2008) Dynamics of dynamin during clathrin mediated endocytosis in PC12 cells. *PloS ONE* **3,** e2416
71. Bossy, B., Petrilli, A., Klinglmayr, E., Chen, J., Lütz-Meindl, U., Knott, A. B., Masliah, E., Schwarzenbacher, R., and Bossy-Wetzel, E. (2010) *S*-nitrosylation of DRP1 does not affect enzymatic activity and is not specific to Alzheimer's disease. *J. Alzheimers Dis.* **20,** S513–S526
72. Lee, Y. C., Taraschi, T. F., and Janes, N. (1993) Support for the shape concept of lipid structure based on a headgroup volume approach. *Biophys. J.* **65,** 1429–1432
73. Chernomordik, L. V., and Kozlov, M. M. (2008) Mechanics of membrane fusion. *Nat. Struct. Mol. Biol.* **15,** 675–683
74. Kozlovsky, Y., and Kozlov, M. M. (2003) Membrane fission: model for intermediate structures. *Biophys. J.* **85,** 85–96
75. Shnyrova, A. V., Bashkirov, P. V., Akimov, S. A., Pucadyil, T. J., Zimmerberg, J., Schmid, S. L., and Frolov, V. A. (2013) Geometric catalysis of membrane fission driven by flexible dynamin rings. *Science* **339,** 1433–1436